# A Computational Study of Electronic and Spectroscopic Properties of Formic Acid Dimer Isotopologues

**M. Mališ, I. Matanović, and N. Došlić***

*Department of Physical Chemistry, R. Bošković Institute, Bijenička 54, 10000, Zagreb, Croatia*

*Received: February 5, 2009; Revised Manuscript Received: April 2, 2009*

We consider the effect of isotopic labeling on the electric charge distribution and dynamics of the formic acid dimer. Our investigation is based on accurate ab initio calculations of vibrationally induced dipole moments and multidimensional quantum calculations of vibrational ground-state splittings. It is found that non-negligible dipole moments of $\mu = 0.032$ D and $\mu = 0.021$ D arise in HCOOH−DOOCD and HCOOH−DOOCH, respectively, suggesting the feasibility of microwave studies. Within the reaction surface Hamiltonian approach a ratio of splittings of 1:0.2:0.045 is predicted for HCOOH−HOOCH:HCOOH−DOOCH:HCOOD−DOOCH.

## I. Introduction

The goal of this paper is to investigate the effect that an asymmetric replacement of hydrogen by deuterium has on the electric charge distribution and dynamics of the formic acid dimer (FAD). From a practical point of view, asymmetric deuterium labeling induces a small but detectable vibrational dipole moment in a molecule that otherwise has no permanent dipole moment. Such labeling, hence, opens the route toward studies in the microwave (MW) region. From a more fundamental point of view, by affecting the size of the tunneling splittings, isotope substitution provides information on the type of dynamics involved. Specifically, in an asymmetrically deuterated dimer of formic acid a change from synchronized to unsynchronized motion of the two hydrogens may occur.

Due to the prototype character of FAD,[1] several experimental[2–6] and theoretical studies[7–12] have focused on obtaining accurate structural and spectroscopical parameters for the regular and symmetrically deuterated dimers. From the experimental side, early electron diffraction work of Almenningen et al.[2] revealed two asymmetric hydrogen bonds with hydrogen bond distances, O−H···O, of 2.703 Å. The rotational constants of DCOOH−HOOCD have been determined by Madeja and Havenith[3] using high-resolution IR spectroscopy and the MP2/TZ2P structure proposed by Neuheuser et al.[8] Rotational parameters for the regular dimer, HCOOH−HOOCH, were obtained by Matylitsky et al.[4] using degenerate four wave mixing and assuming the dimer structure of Chocholoušová et al.[9] and subsequently by Ortlieb et al.[5] Recently, the rotational constants for DCOOD−DOOCD have been reported by Havenith and co-workers.[6] In the case of the regular dimer a very good agreement between the two sets of experimental parameters is found, as well as between the theoretical and experimental structures. Between the latter the largest deviation is found for the *B* constants which reflects the difference in the interoxygen distances between the experimental value of 2.696 Å[5] and the MP2/TZ2P[8] value of 2.672 Å. These experimental data allow us to estimate the reliability of the vibrationally averaged dipole moment calculations in four asymmetrically deuterated dimers: HCOOH−DOOCH, HCOOH−HOOCD, HCOOH−DOOCD, and HCOOD−HOOCD. Here we assume that the dipole moment

in asymmetrical dimers arises solely from the vibrational motion, i.e., from the different composition and anharmonicity of normal modes.

The second part of this work concerns the computation of the vibrational ground-state splittings in formic acid dimer isotopologues. Primarily we focus on HCOOH−DOOCH, a HD transfer system. Unfortunately, there are no measurements of tunneling splittings in any of the three possible HD transfer dimers that would directly address the problem of synchronized versus unsynchronized proton motion. To complete the picture of tunneling in FAD we computed also the ground-state splitting in a double deuterium transfer system for which Havenith and co-workers[6] estimated that the ground-state splitting is below 0.002 cm$^{-1}$.

Taking into account that accurate, full dimensional calculations of the tunneling splittings in FAD are still beyond the reach of quantum dynamics, we shall predict the magnitude of the ground-state splittings by comparing the results obtained by using the reaction surface Hamiltonian (RSH) approach[13–15] on two potential energy surfaces (PES) with experimental data. Previous studies by Barnes et al.[16–18] and Matanović et al.[12,19] on the regular dimer revealed that the three-dimensional (3D) reaction surface dominates the tunneling dynamics. Namely, the exact size of the splittings depends sensitively on the number and symmetry of the bath modes included in the computation, but the contribution of symmetric and antisymmetric modes largely cancels out. For example in HCOOH−HOOCH the ground-state splitting computed on the 3D reaction surface is $\Delta^{3D} = 0.197$ cm$^{-1}$ at the B3LYP/6-311++G(3df,3pd) level of theory, while the splitting computed on a 5D surface involving the two most strongly coupled modes, the symmetric and antisymmetric OH stretchings, is $\Delta^{5D} = 0.170$ cm$^{-1}$. The small difference is a consequence of opposite contributions coming from the suppressing, antisymmetric OH stretch ($\Delta^{4D} = 0.163$ cm$^{-1}$) and promoting, symmetric OH stretch ($\Delta^{4D} = 0.266$ cm$^{-1}$).

Here we consider only the reaction surface dynamics and estimate the actual size of the splittings by comparing results obtained on PES of different quantum chemical levels with available theoretical and experimental data. Within the generalized approximation to the reaction path (GARP) method[19] we spanned the reaction surface by a set of mass weighted internal coordinates known as the Hirschfelder "mobile".[20–22] These are

Properties of Formic Acid Dimer Isotopologues

*J. Phys. Chem. A, Vol. 113, No. 20, 2009* **6035**

obtained via an optimization procedure which minimizes the number of coordinates needed to contain the intrinsic reaction path (IRP) for proton transfer. In all formic acid dimer isotopologues the analysis of the IRP reveals that the two particles are transferred synchronously. In the case of HD transfer, one may question the validity of this assumption, primarily on the grounds of different anharmonic couplings acting on the OH and OD stretches. Here the full dimensionality of ab initio molecular dynamics[23] may help for such calculations do not favor a priori a reaction path. In the case of HCOOH−HOOCH, Markwick et al.[23] have shown that the proton transfer is concerted as obtained from the IRP, but unfortunately there are no Car−Parrinello calculations on HD transfer systems available for comparison. We hope that by combining the theoretical results presented in this paper with MW or IR measurements of the ground-state splittings in HD systems one will be able not only to validate the concerted proton transfer mechanism assumed in this work but also to shed new light on the tunneling dynamics in general.

## II. Electronic Structure Calculations

Within the Born−Oppenheimer approximation the regular and symmetrically deuterated isotopologues of the formic acid dimer have no permanent dipole moments. In asymmetrical iso-topologues such as HCOOH−DOOCH, HCOOH−HOOCD, HCOOD−HOOCD, and HCOOH−DOOCD the electronic dipole moment is vibrationally induced. To compute the vibrationally averaged dipole moments $\langle u \rangle$ a second-order Taylor series expansion with respect to the normal coordinates $Q_i$ is performed

$$\langle u \rangle = \mu_e + \sum_i \left( \frac{\partial \mu}{\partial Q_i} \right) \langle Q_i \rangle + \frac{1}{2} \sum_{ij} \left( \frac{\partial^2 \mu}{\partial Q_i Q_j} \right) \langle Q_i Q_j \rangle \quad (1)$$

The normal mode expectation values $\langle Q_i \rangle$ and $\langle Q_i Q_j \rangle$ are computed using perturbation theory as in refs 24 and 25

$$\langle Q_i \rangle = -\frac{\hbar}{4\omega_i^2} \sum_j \frac{\varphi_{ijj}}{\omega_j} \left( v_j + \frac{1}{2} \right) \quad (2)$$

and

$$\langle Q_i Q_j \rangle = -\frac{\hbar}{2\omega_i} \delta_{ij} \left( v_j + \frac{1}{2} \right) \quad (3)$$

where $\phi_{ijj}$ are cubic anharmonic force constants computed by two points numerical derivation of displaced Hessians. The above procedure is implemented in the Mainz−Austin−Budapest version of ACES II program.[26]

The calculations were performed at the MP2 level of theory with the DZP,[27,28] TZP,[29,30] and cc-pVTZ[31] basis sets. The molecular geometry of the regular dimer (HCOOH)$_2$ was optimized within the constraint of $C_{2h}$ point group symmetry and without it. No difference in the optimized geometries was found. The dipole moments for the four isotopologues were calculated at the optimized geometry. The effects of temperature were accounted for as a rotational contribution to the average value of a normal coordinate $\langle Q_i \rangle$[24] and evaluated at 100, 200, and 300 K.

For the tunneling splitting computations, the 3D PESs for HCOOH−DOOCH and HCOOD−DOOCH were generated by using density functional theory (DFT) with the B3LYP functional and the 6-311++G(3df,3pd) and 6-31+G(d) basis sets as implemented in GAUSSIAN 03.[32] Both basis sets have been used in a number of previous publications[10,12,17,19,33–35] which allows a direct comparison between different methods as well

as an estimate of the splitting in real systems. For the estimate it is important to note that with respect to the reference CCSD(T)/aug-cc-pVTZ//MP2/aug-cc-pVTZ calculation of Tautermann et al.[10] predicting a barrier to proton transfer of $\Delta E = 2763$ cm$^{-1}$ the B3LYP/6-31+G(d) method overestimates the barrier as $\Delta E = 2938$ cm$^{-1}$, while B3LYP/6-311++G(3df,3pd) yields a barrier of only $\Delta E = 2273$ cm$^{-1}$. It is well-known that computed tunneling splittings are very sensitive to the shape of the underlying PES and in particular to the barrier to proton transfer. Hence by selecting the B3LYP functional and the two basis sets we do not attempt to obtain an exact value of the ground-state splitting that can be directly compared to experiment but to provide a lower (B3LYP/6-31+G(d)) and upper (B3LYP/6-311++G(3df,3pd)) bound to the actual splitting. Note that for this reason the barriers to proton transfer have not been corrected for the basis set superposition error (BSSE). In the case of the 6-31+G(d) set, the BSSE correction is quite large and amounts to 431 cm$^{-1}$; i.e., the counterpoint corrected[36] B3LYP/6-31+G(d) barrier is $\Delta E = 2500$ cm$^{-1}$,[11] which is too low for the purpose of our calculation.

## III. Computation of Tunneling Splittings

**III.1. The Choice of Coordinates.** The derivation of the reaction surface Hamiltonian in terms of Hirschfelder "mobile" coordinates has been described in detail in a previous publication.[19] The main features of the method are presented below.

We start by imposing the Eckart conditions to the IRP geometries to approximately separate the vibrational and rotational motion. The goal is to construct a reaction surface of minimum possible dimension that fully contains the IRP.

Mass-weighted vectors $\tilde{\mathbf{S}}_i$ defined as

$$\tilde{S}_{i,\alpha} = \sum_{j=1}^{N} \tilde{W}_{ij} \sqrt{m_j} r_{j\alpha} \quad (4)$$

are a convenient choice for spanning the reaction surface. Here $N$ is the number of atoms, $m_j$ is the mass of the $j$th particle, $\tilde{\mathbf{r}}$ is a $N \times 3$ matrix of Cartesian coordinates, and $\tilde{\mathbf{W}}$ is an orthogonal matrix to be determined. Note also that any unitary transformation applied to a set of vectors $\tilde{\mathbf{S}}_i$ produces another acceptable set of vectors

$$\tilde{S}_i^{\text{new}} = \sum_{j=1}^{N-1} \tilde{A}_{i,j} \tilde{S}_j \quad (5)$$

Thus within an optimization procedure a new, "skewed" set of coordinates, $\tilde{\mathbf{S}}_i^{\text{new}}$ can be obtained in which a smaller number of coordinates may be required to span the reaction surface.
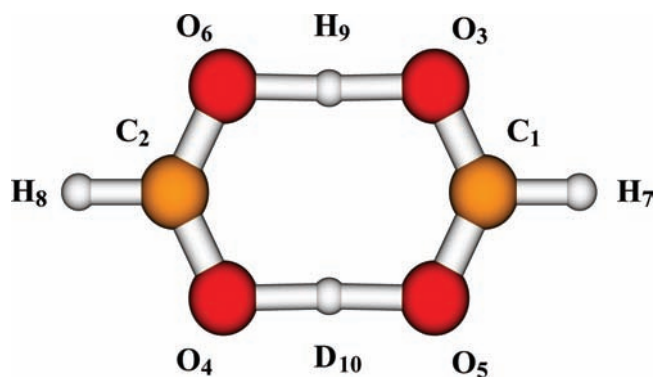


**Figure 1.** Structure of HCOOH−DOOCH at the transition state (B3LYP/6-311++G(3df,3pd)) and numeration of atoms.

Let us now consider a related set of coordinates $Z_i$ defined with respect to the transition state structure. The vector $\mathbf{Z}_N = (Z_{N,x}, Z_{N,y}, Z_{N,z})$ with elements

$$Z_{N,\alpha} = \frac{1}{M_N} \sum_{i=1}^{N} m_i \tilde{r}_{i,\alpha} \tag{6}$$

is fixed and corresponds to the center of mass, while the other $N-1$ vectors can be expressed as

$$Z_{i,\alpha} = \sum_{j=1}^{N} T_{ij} \tilde{r}_{j,\alpha} \tag{7}$$

where $\mathbf{T}$ is an $N \times N$ mass-dependent transformation matrix with elements $T_{N,j} = m_j/M_N$. For HCOOH−DOOCH shown in Figure 1, our initial choice of symmetry adapted coordinates is

$$\mathbf{Z}_1 = \tilde{\mathbf{r}}_1 - \tilde{\mathbf{r}}_2 + \tilde{\mathbf{r}}_8 - \tilde{\mathbf{r}}_7$$

$$\mathbf{Z}_2 = \tilde{\mathbf{r}}_1 + \tilde{\mathbf{r}}_2 - \tilde{\mathbf{r}}_8 - \tilde{\mathbf{r}}_7$$

$$\mathbf{Z}_3 = \tilde{\mathbf{r}}_3 - \tilde{\mathbf{r}}_6$$

$$\mathbf{Z}_4 = \tilde{\mathbf{r}}_5 - \tilde{\mathbf{r}}_4$$

$$\mathbf{Z}_5 = \tilde{\mathbf{r}}_9 - \frac{1}{2}(\tilde{\mathbf{r}}_3 + \tilde{\mathbf{r}}_6)$$

$$\mathbf{Z}_6 = \tilde{\mathbf{r}}_{10} - \frac{1}{2}(\tilde{\mathbf{r}}_4 + \tilde{\mathbf{r}}_5)$$

$$\mathbf{Z}_7 = \frac{\tilde{\mathbf{r}}_1 m_C + \tilde{\mathbf{r}}_7 m_H}{m_C + m_H} - \frac{\tilde{\mathbf{r}}_2 m_C + \tilde{\mathbf{r}}_8 m_H}{m_C + m_H}$$

$$\mathbf{Z}_8 = \frac{\tilde{\mathbf{r}}_3 m_O + \tilde{\mathbf{r}}_6 m_O + \tilde{\mathbf{r}}_9 m_H}{m_H + 2m_O} - \frac{\tilde{\mathbf{r}}_4 m_O + \tilde{\mathbf{r}}_5 m_O + \tilde{\mathbf{r}}_{10} m_D}{m_D + 2m_O}$$

$$\mathbf{Z}_9 = \frac{(\tilde{\mathbf{r}}_3 + \tilde{\mathbf{r}}_4 + \tilde{\mathbf{r}}_5 + \tilde{\mathbf{r}}_6)m_O + \tilde{\mathbf{r}}_9 m_H + \tilde{\mathbf{r}}_{10} m_D}{4m_O + m_H + m_D} -$$
$$\frac{(\tilde{\mathbf{r}}_1 + \tilde{\mathbf{r}}_2)m_C + (\tilde{\mathbf{r}}_7 + \tilde{\mathbf{r}}_8)m_H}{2m_H + 2m_C} \tag{8}$$

The orthogonal vectors $\tilde{\mathbf{S}}$ are now constructed as

$$\tilde{S}_{i,\alpha} = \sqrt{\mu_i} Z_{i,\alpha} \tag{9}$$

where the diagonal matrix $\mu$ given by

$$\mu^{-1} = \mathbf{T}\mathbf{m}^{-1/2}(\mathbf{T}\mathbf{m}^{-1/2})^T \tag{10}$$

is obtained from eqs 9 and 4 and the orthogonality condition $\tilde{\mathbf{W}}\tilde{\mathbf{W}}^T = \mathbf{I}$.

Taking into account that we wish to minimize the number of coordinates required to span the reaction surface and that the double proton transfer in FAD is an in-plane process, it is more convenient to decompose $\tilde{\mathbf{S}}_i$ into components as

$$S_i = \sum_{j}^{3N} W_{ij}\sqrt{m_j} r_j \tag{11}$$

where now the Cartesian coordinates are organized as a $3N$ vector

$$\mathbf{r} = (x_1, x_2, \ldots, x_N, y_1, y_2, \ldots, y_N, z_1, z_2, \ldots, z_N)^T \tag{12}$$

and $\mathbf{W}$ is a corresponding $3N \times 3N$ block diagonal matrix.

**III.2. Construction of the Reaction Surface.** Starting from the initial set of coordinates $S_i$, we derive a new set $S_i^{new}$ tailored to describe the proton transfer reaction. The optimizing proce-

dure is based on a series of kinematic rotations between pairs of coordinates $\tilde{S}_i$ through an angle $\theta$

$$\tilde{S}_i^{(new)} = \tilde{S}_i \cos(\theta) + \tilde{S}_j \sin(\theta)$$

$$\tilde{S}_j^{(new)} = -\tilde{S}_i \sin(\theta) + \tilde{S}_j \cos(\theta) \tag{13}$$

In each rotation the angle $\theta$ is optimized in such a way as to minimize the change of the coordinate $S_i^{(new)}$

$$\min(\max(S_i^{new}(p)) - \min(S_i^{new}(p))) \tag{14}$$

along the $p = 70$ symmetry unique IRP geometries. For each class of vectors 2500 kinematic rotations were performed, with self-consistency reached after $\approx 1100$ rotations. Note that in ref 19 an optimized procedure of kinematic rotations was used to obtain a hierarchically organized set of coordinates, while here a random series of rotations was applied. As for the regular dimer, we found that three coordinates change considerably along the IRP. They are denoted $S_1$, $S_2$, and $S_3$ and span the reaction surface part of the Hamiltonian

$$\hat{H}^{RS} = -\frac{1}{2}\sum_{i=1}^{3}\frac{\partial^2}{\partial S_i^2} + V(S_1, S_2, S_3, \mathbf{S}^B = 0) \tag{15}$$

while the remaining $S_i$, $i = 4, 5, \ldots, 3N - 6$ coordinates that are approximately constant along the IRP constitute the bath and are denoted as $\mathbf{S}^B$.

## IV. Results and Discussion

**IV.1. Rotational Constants and Dipole Moments.** Our first goal is to compute the vibrationally induced dipole moments in four formic acid isotopologues. Due to the numerical effort, i.e., the number of times that the Hessian matrix needs to be calculated in order to obtain full cubic force field (eq 1), the calculations were performed at the MP2 level of theory with moderate basis sets: DZP, TZP, and cc-pVTZ. Hence, in order to validate the results, we first computed the rotational constants of the regular dimer at the same levels of theory and compared them to the experimental values[5] as well as to theoretical rotational constants that so far gave the best overall agreement with the experiment.[6] The latter correspond to the structural parameters obtained by Neuheuser et al.[8] at the MP2/TZ2P level of theory. The orientation of the formic acid dimer in the main axis system is shown in Figure 2, and the results are presented in Table 1. One sees that the ground-state vibrational constants, $X_0$ ($X = A, B, C$) calculated at the MP2/DZP level compare favorably with experiment, with errors of 0.01−0.53%. Larger deviations are found for both the MP2/TZP and MP2/cc-pVTZ results. Of course, the good agreement of MP2/DZP with
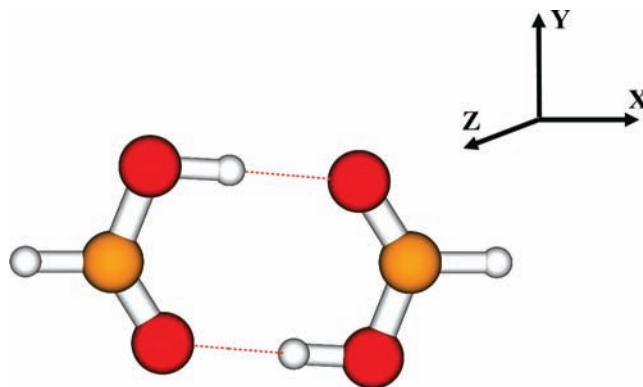


**Figure 2.** Structure of HCOOH−HOOCH at the minimum (MP2/). Principle axes of inertia are displayed.

Properties of Formic Acid Dimer Isotopologues

*J. Phys. Chem. A, Vol. 113, No. 20, 2009* **6037**

**TABLE 1: Calculated Equilibrium, $X_e$, and Ground State, $X_0$, Rotational Constants of the Regular Dimer, HCOOH−HOOCH**

| constant | method | $A$/cm$^{-1}$ | $B$/cm$^{-1}$ | $C$/cm$^{-1}$ |
|---|---|---|---|---|
| $X_e$ | MP2/DZP | 0.20263 | 0.07670 | 0.05564 |
| $X_e$ | MP2/TZP | 0.20280 | 0.07544 | 0.05498 |
| $X_e$ | MP2/cc-pVTZ | 0.20243 | 0.07802 | 0.05631 |
| $X_e$ | MP2/aug-cc-pVTZ | 0.20130 | 0.07712 | 0.05576 |
| $X_e$ | MP2/aug-cc-pVQZ | 0.20243 | 0.07714 | 0.05586 |
| $X_e$ | CCSD(T)/cc-pVTZ | 0.20248 | 0.07728 | 0.05593 |
| $X_0$ | MP2/DZP | 0.20135 | 0.07645 | 0.05541 |
| $X_0$ | MP2/TZP | 0.20153 | 0.07516 | 0.05475 |
| $X_0$ | MP2/cc-pVTZ | 0.20120 | 0.07809 | 0.05627 |
| $X_0$[a] | CCSD(T)/DZP | 0.20120 | 0.07703 | 0.05571 |
| $X_0$[a] | CCSD(T)/TZP | 0.20121 | 0.07701 | 0.05570 |
| $X_0$[a] | CCSD(T)/cc-pVTZ | 0.20125 | 0.07736 | 0.05566 |
| $X_e$ | MP2/TZ2P[b] | 0.20171 | 0.07656 | 0.05550 |
| | experimental[c] | 0.20241 | 0.07635 | 0.05542 |

[a] The CCSD(T) ground-state constants were calculated by using corresponding MP2 ground-state corrections, $X_e - X_0$. [b] Reference 8. [c] Reference 5.

experiment is due to favorable cancelation of errors that appears when MP2 is combined with small basis sets. Further we computed the CCSD(T)/cc-pVTZ equilibrium rotational constants ($X_e$) and converted them to ground-state values by using the vibrational corrections ($X_e - X_0$, $X = A, B, C$) evaluated at the MP2/cc-pVTZ level.[37] From Table 1 it is apparent that the overall agreement with experiment has not been improved and that the MP2/DZP level should provide a reliable estimate of the dipole moment in FAD isotopologues.

Vibrationally averaged dipole moments of the four FAD isotopologues are presented in Table 2. The values $\mu_a$ and $\mu_b$ correspond to the dipole components along the inertial axes $a$ and $b$. It is found that, independently of the level of computation, the dipole moment decreases in the order $\mu$(HCOOH−DOOCD) > $\mu$(HCOOH−DOOCH) > $\mu$(HCOOH−HOOCD) ≈ $\mu$(HCOOD−HOOCD). Comparing different basis sets we see a difference of ≈20% in the values of the dipole moments with TZP predicting consistently smaller and cc-pVTZ larger dipole moments. Specifically, for HCOOH−DOOCD total dipole moments, $\mu$, of 0.0322, 0.0280, and 0.0374 D are found at the MP2/DZP, TZP, and cc-pVTZ levels, respectively. The largest dipole component is directed along the $a$ axis, i.e., in the proton transfer direction.

At vibrationally averaged geometries the dipole moments are negligible. Hence, in FAD dimers as in other molecules with no permanent dipole moment, the dipole comes from the derivatives of $\mu$ along the normal modes.[38] Inspection of the individual normal mode contributions reveals the modes that are responsible for the onset of the dipole moment. As expected, the largest contribution arises from the difference between the dipole moments along the OH and OD stretching normal modes. These are strongly anharmonic vibrations sensitive to isotope substitution. In the monodeuterated HCOOH−DOOCH the
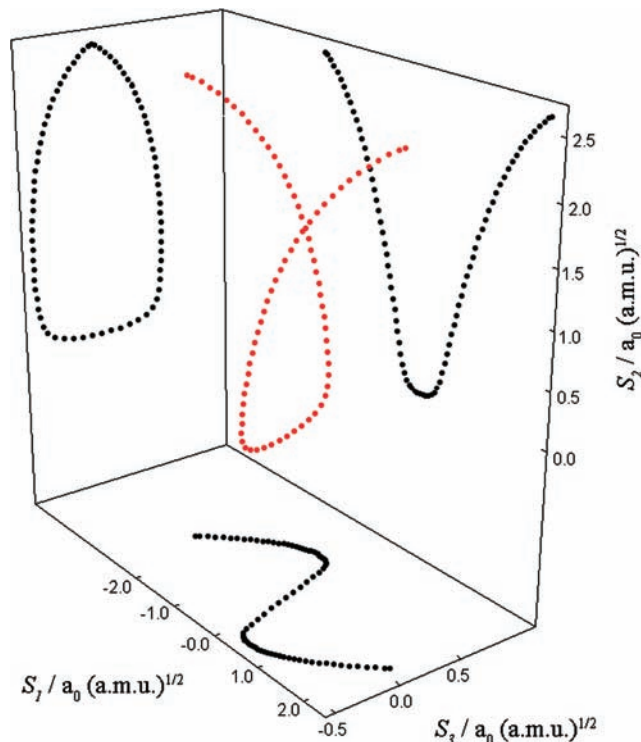


**Figure 3.** Projection of the IRP of HCOOH−DOOCH on the 3D reaction surfaces ($S_1$, $S_2$, $S_3$) and changes of the reaction coordinates along the IRP.

$\nu$(OH) and $\nu$(OD) stretching contributions to the total dipole moment are 0.0617D and −0.0502 D (MP2/cc-pVTZ), respectively. On the contrary, in HCOOH−HOOCD where the dipole moment arises from the $\nu$(CH) and $\nu$(CD) stretchings these contributions are much smaller being $\mu_{CH} = 0.0151$ D and $\mu_{CD} = -0.0119$ D. It is clear that HCOOH−DOOCD and HCOOD−HOOCD contain the four modes that contribute most to the onset of the dipole moment. The total dipole moment is maximized in HCOOH−DOOCD where the dipoles arising from the difference of the OH/OD and CH/CD contributions sum up, whereas it is minimized in HCOOD−HOOCD where these contributions cancel out. Regarding temperature effects, due to compensation of rotational and vibrational effects in HCOOH−DOOCD and HCOOH−HOOCD the dipole moment values changes slightly, by ≈6% over a 300 K temperature range whereas it increases by 15% and 20% in HCOOH−DOOCH and HCOOD−HOOCD, respectively.

We conclude this section by noting that the vibrationally induced dipole moment in HCOOH−DOOCD has a small, but non-negligible magnitude. The values of $\mu = 0.0322$ D and $\mu_a = 0.0317$ suggest that it is feasible to recover the rotational spectrum of the dimer and directly measure the splitting of the ground-state levels.

**IV.2. Ground-State Tunneling Splittings.** Let us now focus on tunneling. Figure 3 displays the projections of the IRP on

**TABLE 2: Dipole Moment Values at Various Levels of Theory[a]**

| | MP2/DZP | | | MP2/TZP | | | MP2/cc-pVTZ | | |
|---|---|---|---|---|---|---|---|---|---|
| dimer | $\mu_a$ | $\mu_b$ | $\mu$ | $\mu_a$ | $\mu_b$ | $\mu$ | $\mu_a$ | $\mu_b$ | $\mu$ |
| HCOOH−DOOCD | 0.0317 | 0.0056 | 0.0322 | 0.0275 | 0.0052 | 0.0280 | 0.0371 | 0.0045 | 0.0374 |
| HCOOH−DOOCH | 0.0194 | 0.0070 | 0.0206 | 0.0164 | 0.0068 | 0.0178 | 0.0250 | 0.0061 | 0.0258 |
| HCOOH−HOOCD | 0.0121 | −0.0011 | 0.0121 | 0.0109 | −0.0015 | 0.0110 | 0.0119 | −0.0014 | 0.0120 |
| HCOOD−HOOCD | 0.0074 | 0.0080 | 0.0109 | 0.0056 | 0.0081 | 0.0098 | 0.01312 | 0.0074 | 0.0150 |

[a] Values in Debye at $T = 0$ K.
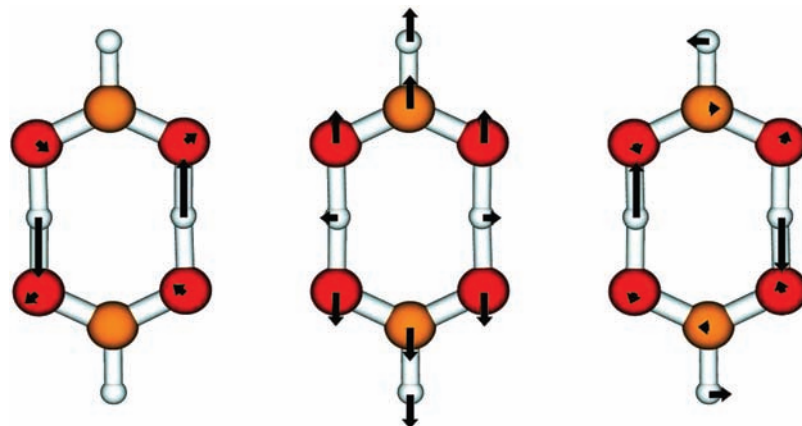
**Figure 4.** The Cartesian displacement vectors corresponding to the mass-weighted internal coordinates $S_1$, $S_2$, and $S_3$.
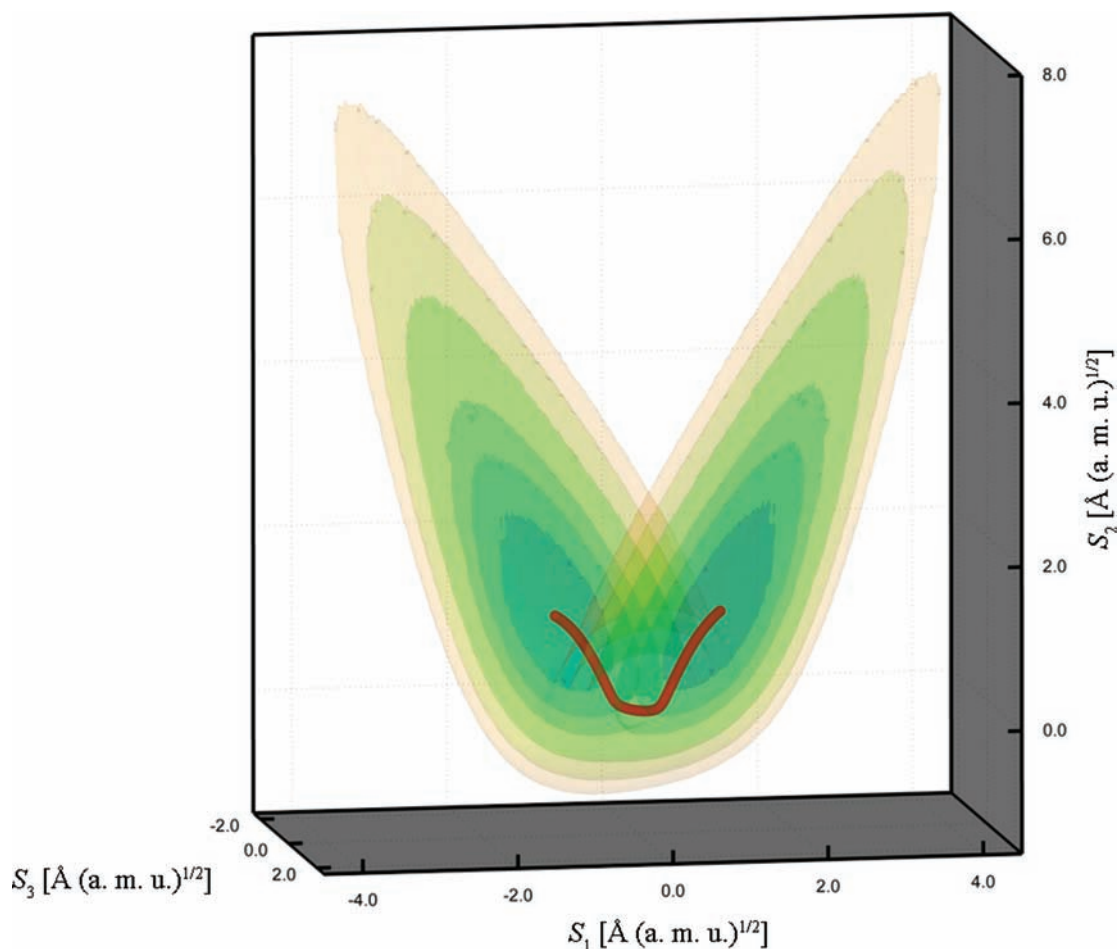


**Figure 5.** The 3D reaction surface $V(S_1, S_2, S_3)$ for double deuterium transfer in HCOOD−DOOCH and the corresponding IRP (solid line). The coordinates are in $a_0$(a.m.u.)$^{1/2}$. The innermost contour is at 806.5 cm$^{-1}$, the outermost at 7259 cm$^{-1}$, and the spacing is 806.5 (1613) cm$^{-1}$ between the three inner (outer) contours.

the 3D reaction surfaces $(S_1, S_2, S_3)$ for HCOOH−DOOCH together with the changes of the reaction coordinates along the IRP. The Cartesian displacement vectors corresponding to the internal coordinates $S_i$ are shown in Figure 4. The three vectors have $C_S$ symmetry with $S_1$ and $S_3$ being antisymmetric and $S_2$ being symmetric with respect to HD transfer. On the first glance it is apparent that the changes of $S_1$, $S_2$, and $S_3$ in HCOOH−DOOCH are very similar to those in HCOOH−-HOOCH.[19] However, when analyzing the Cartesian displacements of the three $S_i$ coordinates (eq 11), we see that the random kinematic rotation procedure leads to asymmetric coordinates $S_1$ and $S_3$

that both decompose into a HD transfer contribution and a contribution from the rearrangement of the molecular frame.

To assess the quality of the 3D reaction surfaces constructed using the optimization procedure described in section III.2, we computed the root-mean-square (rms) deviation between the IRP geometries and their projection on the 3D reaction surface[12,39] spanned by $(S_1, S_2, S_3)$. By definition the rms difference vanishes at the transition state ($p = 0$). For the asymmetrically deuterated dimer HCOOH−DOOCH at the B3LYP/6-311++G(3df,3pd) level the rms difference at the minimum, $p = \pm 3.4a_0$ (a.m.u.)$^{1/2}$ is below 1 cm$^{-1}$ while a maximum deviation corresponding to

Properties of Formic Acid Dimer Isotopologues

*J. Phys. Chem. A, Vol. 113, No. 20, 2009* **6039**

**TABLE 3: Computed and Experimental Tunneling Splittings for Different FAD Isotopologues**

| transferring particles | method | $\Delta E/cm^{-1}$ |
|---|---|---|
| HD | B3LYP/6-311++G(3df,3pd) | 0.038621 |
| HD | B3LYP/6-31+G(d) | 0.000627 |
| HD | estimate | 0.003 |
| DD | B3LYP/6-311++G(3df,3pd) | 0.008996 |
| DD[a] | experiment | <0.002 |
| DD | estimate | 0.0007 |
| HH[b] | B3LYP/6-311++G(3df,3pd) | 0.1970 |
| HH[b] | B3LYP/6-31+G(d) | 0.0032 |
| HH[c] | experiment | 0.0158 |

[a] Reference 6. [b] Reference 12. [c] Reference 3.

30 cm$^{-1}$ is found for the geometries at $p = \pm 2.1 a_0$ (a.m.u.)$^{1/2}$. The deviation between the IRP and its projection is negligible when compared to the B3LYP/6-311++G(3df,3pd) barrier to proton transfer of $\Delta E = 2273$ cm$^{-1}$. However, the error is larger than the maximum energy difference of $\Delta_{IRP} = 7$ cm$^{-1}$ found between the IRPs of the mono- and dideuterated dimers, HCOOH−DOOCH and HCOOH−DOOCD. In other words, within the 3D reaction surface the two species are indistinguishable and in order to distinguish between them the normal modes corresponding to C−H/C−D stretchings and/or bendings need to be explicitly included in the Hamiltonian. From the experiments of Havenith and co-workers[3,5] we know that the replacement of hydrogen by deuterium in the C−H bonds causes a reduction of the ground-state splitting by ≈20%, from $\Delta = 0.0158$ cm$^{-1}$ in HCOOH−HOOCH to $\Delta = 0.0125$ cm$^{-1}$ in DCOOH−HOOCD. In the present investigation we are concerned with larger effects for the replacement of one or both bridging hydrogens is expected to affect the ground-state splittings by more than an order of magnitude.

The ground-state splitting is calculated as the difference between the two lowest eigenvalues of the Hamiltonian given in eq 15. To achieve convergence of the splittings the $V(S_1, S_2, S_3)$ surfaces were generated on the basis of 1549 symmetry unique single energy points, gradients, and Hessians for HCOOH−DOOCH and 1839 for HCOOD−DOOCH. In both cases the PES were interpolated using the weighted Shepard interpolation scheme[39] on a $85 \times 93 \times 39$ grid in the range ($a_0$ (a.m.u.)$^{1/2}$): $-7.600 \leq S_1 \leq 7.600$, $-2.100 \leq S_2 \leq 14.500$, $-3.150 \leq S_3 \leq 3.150$ for HCOOH−DOOCH and $-7.650 \leq S_1 \leq 7.650$, $-1.900 \leq S_2 \leq 14.600$, $-3.500 \leq S_3 \leq 3.500$. The 3D reaction surface $V(S_1, S_2, S_3)$ for HCOOD−DOOCH exhibiting a characteristic butterfly shape is shown in Figure 5. The time-independent Schrödinger equation was solved using the grid Hamiltonian method[40,41] combined with the implicitly restarted Lanczos diagonalization method[42] as implemented in the ARPACK code.[43,44]

Table 3 compiles the tunneling splittings of HCOOH−DOOCH and HCOOD−DOOCH and compares them to corresponding theoretical and available experimental results. As expected,[12] a strong basis set dependence of the ground-state splittings is found, because the PES computed at the B3LYP/6-311++G(3df,3pd) and B3LYP/6-31+G(d) levels are characterized by very different barriers to proton transfer, of 2273 and 2938 cm$^{-1}$, respectively. The computed ground-state splittings thus provide an upper and a lower bound for the actual splitting, in the same way as the two HH splittings of ref 12 computed on the same levels of theory compare to the experimental value of Ortlieb and Havenith.[5] Here we take advantage of the constancy of the ratio between the splittings $\Delta_{B3LYP/6-31+G(d)}/\Delta_{B3LYP/6-311++G(3df,3pd)}$ of 0.01624 for HH and 0.01623 for HD

to estimate the actual splitting in HD. On the basis of the assumption that the tunneling dynamics is well described by the reaction space $V(S_1, S_2, S_3)$ encompassing the IRP, we estimate the splitting in HD as $\Delta = 0.003$ cm$^{-1}$. This result finds good agreement with the B3LYP/6-31+G(d) instanton tunneling splitting of $\Delta = 0.0025$ cm$^{-1}$ obtained by Smedarchina et al.[33] Note also that according to our result the HD splitting can be resolved in IR high-resolution experiments.[6]

In HCOOD−DOOCH the two moieties are embedded in an equivalent anharmonic coupling environment where one expects a larger cancelation of promoting and hindering bath mode contributions than in the HD case. For DD tunneling the splitting has been computed at the B3LYP/6-311++G(3df,3pd) level only, and a splitting of 0.008996 cm$^{-1}$ has been obtained. We expect the splitting at the B3LYP/6-31+G(d) to be smaller by approximately an order of magnitude and hence on the border of accuracy of the present calculation. Assuming a ratio of 12.468 for the computed versus measured splitting, as in the HH case, an estimate of $\Delta = 0.0007$ cm$^{-1}$ for the ground-state splitting has been obtained. This prediction is in accord with the estimate of Guberlet et al.[6] of a splitting below 0.002 cm$^{-1}$, as well as with the instanton result of Smedarchina et al.[33]

## V. Conclusion

A combined electronic structure and multidimensional quantum dynamical investigation of several formic acid dimer isotopologues is presented.

It has been shown that the vibrationally induced dipole moment in four asymmetrically deuterated dimers decreases in the order $\mu(HCOOH−DOOCD) > \mu(HCOOH−DOOCH) > \mu(HCOOH−HOOCD) \approx \mu(HCOOD−HOOCD)$. The value of $\mu = 0.032$ D (MP2/DZP) obtained for HCOOH−DOOCD is small, but non-negligible, and indicates that it may be feasible to observe the rotational spectrum of the dimer.

We applied the GARP method to study the ground-state splitting in HCOOH−DOOCH and HCOOD−DOOCH. On the basis of a series of 3D reaction surface calculations a ratio of splitting 1:0.20:0.045 was obtained for $\Delta(HCOOH−HOOCH)$: $\Delta(HCOOH−DOOCH):\Delta(HCOOD−DOOCH)$. The ratio was obtained under the assumption that the tunneling dynamics is dominated by a low dimensional reaction surface constructed around the IRP for hydrogen/deuterium transfer. In all cases the IRP corresponds to a synchronized motion of the transferring particles. We hope that our results will stimulate new experimental and full-dimensional theoretical investigations that could assess the validity of this assumption.

**References and Notes**

(1) Birer, Ö.; Havenith, M. *Annu. Rev. Phys. Chem.* **2009**, *60*, 263.
(2) Almenningen, A.; Bastiansen, O.; Motzfeld, T. *Acta Chem. Scand.* **1969**, *23*, 2848.
(3) Madeja, F.; Havenith, M. *J. Chem. Phys.* **2002**, *117*, 7162.
(4) Matylitsky, V. V.; Reihn, C.; Gelin, M. F.; Brutschy, B. *J. Chem. Phys.* **2003**, *119*, 10553.
(5) Ortlieb, M.; Havenith, M. *J. Phys. Chem. A* **2007**, *111*, 7355.
(6) Gutberlet, A.; Scwaab, G. W.; Havenith, M. *Chem. Phys.* **2008**, *343*, 158.
(7) Juršić, B. S. *J. Mol. Struct.* **1997**, *417*, 89.
(8) Neuheuser, T.; Hess, B. A.; Reutel, C.; Weber, E. *J. Phys. Chem.* **1994**, *98*, 6459.
(9) Chocholoušavá, J. *J. Chem. Phys.* **2000**, *112*, 2655.
(10) Tautermann, C. S.; Voegele, A. F.; Liedl, K. R. *J. Chem. Phys.* **2004**, *120*, 631.
(11) Matanović, I.; Došlić, N. *Chem. Phys.* **2007**, *338*, 121.

(12) Matanović, I.; Došlić, N.; Kühn, O. *J. Chem. Phys.* **2007**, *127*, 014309.

(13) Carrington, T.; Miller, W. H. *J. Chem. Phys.* **1986**, *84*, 4364.

(14) Shida, N.; Barbara, P. F.; Almlöf, J. E. *J. Chem. Phys.* **1989**, *91*, 4061.

(15) Shida, N.; Barbara, P. F.; Almlöf, J. E. *J. Chem. Phys.* **1991**, *94*, 3633.

(16) Barnes, G. L.; Squires, S. A.; Sibert III, E. L. *J. Phys. Chem. B* **2008**, *129*, 164317.

(17) Barnes, G. L.; Sibert, E. L., III. *J. Chem. Phys.* **2008**, *112*, 595.

(18) Barnes, G. L.; Sibert, E. L., III. *J. Mol. Spectrosc.* **2008**, *249*, 78.

(19) Matanović, I.; Došlić, N.; Johnson, B. R. *J. Chem. Phys.* **2007**, *128*, 084103.

(20) Hirschfelder, J. O.; Dahler, J. S. *Proc. Natl. Acad. Sci.U.S.A.* **1956**, *42*, 363.

(21) Hirschfelder, J. O. *Int. J. Quantum Chem.* **1969**, *3*, 17.

(22) Smith, F. T. *J. Chem. Phys.* **1959**, *31*, 1352.

(23) Markwick, P. R. L.; Doltsinis, N. L.; Marx, D. *J. Chem. Phys.* **2005**, *122*, 054112.

(24) Toyama, M.; Oka, T.; Morino, Y. *J. Mol. Spectrosc.* **1964**, *13*, 193.

(25) Russel, A. J.; Spackman, M. A. *Mol. Phys.* **1995**, *84*, 1239.

(26) Stanton, J.; Gauss, J.; Watts, J.; et al., ACES2 (Mainz−Austin−Budapest version), a quantum-chemical program package for high-level calculations of energy and properties, http://www.aces2.de.

(27) Dunning, T. *J. Chem. Phys.* **1970**, *53*, 2823.

(28) Redmon, L.; Purvis, G.; Bartlett, R. *J. Am. Chem. Soc.* **1979**, *101*, 2856.

(29) Dunning, T. *J. Chem. Phys.* **1971**, *55*, 716.

(30) Gauss, J.; Stanton, J.; Bartlett, R. *J. Chem. Phys.* **1992**, *97*, 7825.

(31) Dunning, T. *J. Chem. Phys.* **1989**, *90*, 1007.

(32) Frisch, M. J.; Trucks, G. W.; Schlegel, H. B.; Scuseria, G. E.; Robb, M. A.; Cheeseman, J. R.; Montgomery, J. A., Jr.; Vreven, T.; Kudin, K. N.; Burant, J. C.; Millam, J. M.; Iyengar, S. S.; Tomasi, J.; Barone, V.; Mennucci, B.; Cossi, M.; Scalmani, G.; Rega, N.; Petersson, G. A.; Nakatsuji, H.; Hada, M.; Ehara, M.; Toyota, K.; Fukuda, R.; Hasegawa, J.; Ishida, M.; Nakajima, T.; Honda, Y.; Kitao, O.; Nakai, H.; Klene, M.; Li, X.; Knox, J. E.; Hratchian, H. P.; Cross, J. B.; Adamo, C.; Jaramillo, J.; Gomperts, R.; Stratmann, R. E.; Yazyev, O.; Austin, A. J.; Cammi, R.; Pomelli, C.; Ochterski, J. W.; Ayala, P. Y.; Morokuma, K.; Voth, G. A.; Salvador, P.; Dannenberg, J. J.; Zakrzewski, V. G.; Dapprich, S.; Daniels, A. D.; Strain, M. C.; Farkas, O.; Malick, D. K.; Rabuck, A. D.; Raghavachari, K.; Foresman, J. B.; Ortiz, J. V.; Cui, Q.; Baboul, A. G.; Clifford, S.; Cioslowski, J.; Stefanov, B. B.; Liu, G.; Liashenko, A.; Piskorz, P.; Komaromi, I.; Martin, R. L.; Fox, D. J.; Keith, T.; Al-Laham, M. A.; Peng, C. Y.; Nanayakkara, A.; Challacombe, M.; Gill, P. M. W.; Johnson, B.; Chen, W.; Wong, M. W.; Gonzalez, C.; Pople, J. A. *Gaussian 03, Revision B.05*; Gaussian, Inc.: Wallingford, CT, 2003.

(33) Smedarchina, Z.; Fernandez-Ramos, A.; Siebrand, W. *J. Chem. Phys.* **2005**, *122*, 4309.

(34) Mil'nikov, G. V.; Kühn, O.; Nakamura, H. *J. Chem. Phys.* **2005**, *123*, 074308.

(35) Luckhaus, D. *J. Phys. Chem. A* **2006**, *110*, 3151.

(36) Boys, S. F.; Bernardi, F. *Mol. Phys.* **1970**, *19*, 553.

(37) Breidung, J.; Demaison, J.; D'Eu, J. F.; Margulès, L.; Collet, D.; Mkadmi, E. B.; Perrin, A.; Thiel, W. *J. Mol. Spectrosc.* **2004**, *228*, 7.

(38) Puzzarini, C.; Taylor, P. R. *J. Chem. Phys.* **2005**, *122*, 054315.

(39) Giese, K.; Kühn, O. *J. Chem. Phys.* **2005**, *123*, 054315.

(40) Marston, C. C.; Balint-Kurti, G. *J. Chem. Phys.* **1989**, *91*, 3571.

(41) Stare, J.; Balint-Kurti, G. G. *J. Phys. Chem.* **2003**, *107*, 7204.

(42) Golub, G. H.; Loan, C. F. V. *Matrix Computations*; The Johns Hopkins University Press: Baltimore, MD, 1985.

(43) Sorensen, D. *Tutorial: Implicitly Restarted Arnoldi/Lanczos Methods for Large Scale Eigenvalue Calculations*; Rice University: Houston, TX, 1995.

(44) Lehoucq, R. B.; Sorensen, D.; Yang, C. D. *ARPACK User's Guide: Solution of Large Scale Eigenvalue Problems with Implicitly Restarted Arnoldi Methods*; Rice University: Houston, 1997.